Chromophore switch from 11-*cis*-dehydroretinal (A2) to 11-*cis*-retinal (A1) decreases dark noise in salamander red rods

Petri Ala-Laurila[1], Kristian Donner[2], Rosalie K. Crouch[3] and M. Carter Cornwall[1]

[1]*Department of Physiology and Biophysics, Boston University School of Medicine, Boston, MA, USA*
[2]*Department of Biological and Environmental Sciences, University of Helsinki, Finland*
[3]*Department of Ophthalmology, Medical University of South Carolina, Charleston, SC, USA*

Dark noise, light-induced noise and responses to brief flashes of light were recorded in the membrane current of isolated rods from larval tiger salamander retina before and after bleaching most of the native visual pigment, which mainly has the 11-*cis*-3,4-dehydroretinal (A2) chromophore, and regenerating with the 11-*cis*-retinal (A1) chromophore in the same isolated rods. The purpose was to test the hypothesis that blue-shifting the pigment by switching from A2 to A1 will decrease the rate of spontaneous thermal activations and thus intrinsic light-like noise in the rod. Complete recordings were obtained in five cells (21°C). Based on the wavelength of maximum absorbance, $\lambda_{max,A1} = 502$ nm and $\lambda_{max,A2} = 528$ nm, the average A2 : A1 ratio determined from rod spectral sensitivities and absorbances was ∼0.74 : 0.26 in the native state and ∼0.09 : 0.91 in the final state. In the native (A2) state, the single-quantum response (SQR) had an amplitude of 0.41 ± 0.03 pA and an integration time of 3.16 ± 0.15 s (mean ± S.E.M.). The low-frequency branch of the dark noise power spectrum was consistent with discrete SQR-like events occurring at a rate of 0.238 ± 0.026 rod^{-1} s^{-1}. The corresponding values in the final state were 0.57 ± 0.07 pA (SQR amplitude), 3.47 ± 0.26 s (SQR integration time), and 0.030 ± 0.006 rod^{-1} s^{-1} (rate of dark events). Thus the rate of dark events per rod and the fraction of A2 pigment both changed by *ca* 8-fold between the native and final states, indicating that the dark events originated mainly in A2 molecules even in the final state. By extrapolating the linear relation between event rates and A2 fraction to 0% A2 (100% A1) and 100% A2 (0% A1), we estimated that the A1 pigment is at least 36 times more stable than the A2 pigment. The noise component attributed to discrete dark events accounted for 73% of the total dark current variance in the native (A2) state and 46% in the final state. The power spectrum of the remaining 'continuous' noise component did not differ between the two states. The smaller and faster SQR in the native (A2) state is consistent with the idea that the rod behaves as if light-adapted by dark events that occur at a rate of nearly one per integration time. Both the decreased level of dark noise and the increased SQR amplitude must significantly improve the reliability of photon detection in dim light in the presence of the A1 chromophore compared to the native (A2) state in salamander rods.

(Resubmitted 13 August 2007; accepted after revision 18 September 2007; first published online 20 September 2007)
Corresponding author P. Ala-Laurila: Department of Physiology and Biophysics, Boston University School of Medicine, Boston, MA, USA. Email: pal@bu.edu

Thermal activations of visual pigment molecules in retinal rods trigger discrete electrical 'dark' events that are identical to responses to single photons (Baylor *et al.* 1980, 1984). Such randomly occurring events constitute an irreducible background noise that sets an ultimate limit to visual sensitivity (Barlow, 1956; Aho *et al.* 1988, 1993). Between-species comparisons indicate that long-wavelength sensitivity of visual pigments (i.e. the capacity to be activated by low-energy photons) is, on average, associated with high rates of thermal activations (Ala-Laurila *et al.* 2004*a*,*b*). Spectral tuning of rod pigments for good performance in dim light must then be understood not only in terms of quantum catch, but also in terms of noise control. Indeed, rod pigments tend to be significantly blue-shifted ('Purkinje shift') from the position that would maximize quantum catch (Barlow, 1957; Lythgoe, 1988). Present evidence for this, however, is wholly based on correlation across different photoreceptors.

 DOI: 10.1113/jphysiol.2007.142935

Our purpose was to study, in single isolated salamander rods, how dark noise changes when the visual pigment is spectrally shifted by exchanging the chromophore within these same rods. Vertebrate visual pigments use either 11-*cis*-retinal (A1) or 11-*cis*-3,4-dehydroretinal (A2). In all pigments in the Rh1 pigment family, the wavelength of maximum absorption is shorter when the opsin is bound to the A1 chromophore rather than the A2 form (Dartnall & Lythgoe, 1965). In order to exchange the chromophore, we bleached most of the native A2 visual pigment and then regenerated with the A1 chromophore. This allowed us to evaluate flash sensitivity and membrane current noise in darkness in a single cell with a single opsin in two different conditions. We find that the thermal stability of the 502 nm A1 pigment is over 36-fold greater than the thermal stability of the 528 nm A2 pigment. This suggests that the A1 pigment can support a higher absolute sensitivity of vision than the A2 pigment, since fewer photons will suffice to produce a criterion signal-to-noise ratio.

Methods

Animals and preparation

The experiments were done on isolated red rods of larval tiger salamander *Ambystoma tigrinum* (Charles D. Sullivan Company, Nashville, TN, USA). All procedures were performed according to protocols approved by the Animal Care and Use Committee of Boston University School of Medicine and in accordance with the standards set forth in the *Guide for the Care and Use of Laboratory Animals* (ISBN: 978-0-309-05377-8) and the Animal Welfare Act (http://www.nal.usda.gov/awic/legislat/usdaleg1.htm).

Salamanders were kept at *ca* 10°C in aquarium tanks on a 12 h–12 h light–dark cycle. Animals were dark-adapted overnight before each experiment. The animal to be used in an experiment was decapitated and double-pithed under dim red light. The eyes were enucleated and hemisected and the retinas were isolated in Ringer solution. All subsequent procedures were carried out under infrared illumination with the aid of infrared image converters (Find-R-Scope). Rods were isolated by teasing pieces of retina apart in *ca* 1 ml of Ringer solution. The sample was placed on the stage of an inverted microscope (Invertascope D; Carl Zeiss, Inc.) in a light-tight Faraday cage for electrical recordings. Cells were viewed via a high sensitivity CCD camera (LCL-902HS; Watec) connected to a TV monitor. The video signal was also fed to a computer equipped with a frame grabber card (WinTV-PVR-250, Hauppauge) to capture and store bright-field images of the cells. Cells were superfused by standard Ringer solution (pH 7.8) of the following composition: (mM): 110 NaCl, 2.5 KCl, 1.6 $MgCl_2$, 1.0 $CaCl_2$, 10 dextrose, 10 Hepes; plus 1.5 μM bovine serum albumin. The room temperature was maintained at 21 ± 1°C and monitored throughout the experiment.

Light stimulation

Unpolarized light stimuli were provided from a dual-beam optical stimulator equipped with a tungsten–halogen light source. Computer-controlled shutters (Vincent Associates) were used to deliver 20 ms flashes as well as continuous background illumination and bleaching exposures. The light intensity was controlled by a set of calibrated neutral density filters. The wavelength of light stimuli over the range 400–760 nm was set by interference filters placed in the light beam. Individual filters had a nominal half-bandwidth of 10 nm (Chroma Technology, Rockingham, VT, USA). The unattenuated intensity of a uniform circular spot (diameter, 900 μm) of the stimulus light (540 nm) focused on the plane of the specimen holder was adjusted at the beginning of each experiment to be 1.21×10^8 photons μm^{-2} s^{-1}. This intensity was checked again at the end of each experiment. Light intensities were measured for different combinations of interference filters and neutral density filters used in the experiment by a calibrated radiometer (Model 350; UDT Instruments) placed on the microscope stage at the same level as the preparation.

Light intensities were expressed as rates or numbers of photoisomerizations per rod based on two calibration principles described below in the section on single-photon response analysis. One is based on the response ensemble variance-to-mean ratio obtained from responses to a sequence of very dim flashes, the other on estimations made from OS geometry, pigment density and photon flux. We denote numbers of isomerizations by Rh*. When referring to isomerizations *per rod*, Rh* is used without specification; when referring to isomerizations *per molecule of visual pigment*, this is specified (Rh* molecule^{-1}).

Visual pigment bleaching and regeneration

After the stable dark-adapted 'native' state of a rod had been thoroughly characterized, the cell was bleached by a 30 s exposure to very bright light (520 nm, 1.1×10^7 photons μm^{-2} s^{-1}).

The wavelength used for bleaching, 520 nm, was originally chosen just because it is quite close to the λ_{max} of the native pigment and our bleaching protocols had previously been optimized for this wavelength. Beyond that, it has no special meaning, as opposed to the stimulus wavelength, 540 nm, which was chosen because it is close to the isosbestic point of salamander A1 and A2 pigments and thus stimulates both with the same probability (see further below). As there would have been no specific advantage in

bleaching equal fractions of native A2 and A1 pigment, however, we found no compelling reason to switch to 540 nm for the bleaching light.

The light intensity used for bleaching was *ca* 10 times lower than the maximum available from our light source, because we noticed that the probability of successful regeneration was higher with the lower intensity and longer exposure time than when the same fractional bleach was produced with the maximum intensity and shorter exposure time. We can only speculate on the reasons for this difference. Very intense bleaching might generate a large amount of reactive all-*trans*-retinal, which may compromise the physiological condition of the cell. It is also possible that it generates a larger fraction of long-lasting photoproducts, e.g. metarhodopsin III, where the chromophore binding site is occupied and does not allow the regeneration of the visual pigment with 11-*cis*-retinal. The amount of metarhodopsin III may depend on the intensity of the light used for bleaching as well as its wavelength (Ritter *et al.* 2007). The light exposure was set to bleach a fraction $F \approx 0.9$ of the native pigment according to the relation: $F = 1 - \exp(-IP_\lambda t)$, where I is the bleaching light intensity (photons μm^{-2} s^{-1}), P_λ is the pigment's photosensitivity at the wavelength of stimulus light (μm^2), and t the duration of the exposure (s). For P_λ (520 nm), we used the value 6.2×10^{-9} μm^2 (Jones, 1995). More accurate estimates of the pigment composition before and after bleaching and regeneration were based on spectral sensitivity measurements as explained below.

In the microspectrophotometry, we tested regeneration after even stronger bleaches, exposing the cells for 20 min to a lower light intensity. The combination of relatively low intensity and long exposure time enabled practically complete regeneration with the A1 chromophore even after having bleached 99% of the native pigment (see Fig. 1*B*). However, such very long and strong bleaches were not tried in the electrophysiological experiments.

We used 11-*cis*-retinal (chromophore A1) to regenerate the visual pigment of the bleached rods. The retinoids were synthesized and purified in the Department of Ophthalmology at the Medical University of South Carolina (for review, see Crouch *et al.* 2002). The retinoid solution was prepared as described earlier (Estevez *et al.* 2006) by adding 3 μl ethanol into 50 μg 11-*cis*-retinal (24 900 M^{-1} cm^{-1} at 380 nm) and diluting this solution into *ca* 1 ml of Ringer solution. The final concentration of the retinoid solution was measured in a spectrophotometer (U-3010; Hitachi) to be in the range 40–50 μM in Ringer solution with *ca* 0.3% ethanol. When the cell had settled into a new bleach-adapted steady state *ca* 80 min after the bleach (cf. Fig. 2 below), the gravity-controlled perfusion was stopped and the retinoid solution was added to the specimen chamber. After 20 min of incubation, perfusion was restarted and the retinoid was washed out of the chamber.

Suction electrode recordings in single rods

The membrane current of isolated rods was recorded by drawing the inner segment into a tight-fitting glass micropipette filled with Ringer solution, connected to a patch-clamp amplifier (EPC-7, List Associates) (Baylor *et al.* 1979*a*; Cornwall *et al.* 2000). Pipettes were fire-polished to an internal diameter of *ca* 12 μm and silanized. The resistance was typically *ca* 1 MΩ (open pipette) and *ca* 3 MΩ with a cell drawn into the pipette. Signals were low-pass filtered at 20 Hz with an 8-pole active Bessel filter, digitized at 100 Hz (Digidata 1322A; Axon Instruments) and stored on a computer hard-drive. pCLAMP software components (version 9.2, Axon Instruments) were used for data acquisition and analysis. The recordings were conducted in complete darkness save for the epochs of light flashes, dim backgrounds and saturating light that were part of the experimental protocol. The position of the cell within the micropipette was monitored between recording periods throughout the experiment by capturing bright-field images of the cell under infrared illumination.

Fractional sensitivity and light-sensitive current

The photosensitivity and the maximum response amplitude of the rod were probed at regular intervals throughout the experiments by measuring the response–intensity relation of the rod. The stimulus wavelength, 540 nm, was chosen since it is close to the isosbestic point (537 nm), where the mean number of photoisomerizations produced is independent of the A1/A2 pigment ratio (Cornwall *et al.* 2000). We measured photoresponses to a series of 20 ms flashes at five to six intensities increasing in *ca* 0.5 log unit steps. At each intensity, 1–30 responses were recorded and averaged. The amplitudes of the averaged responses were plotted against flash intensity and fitted by the Michaelis equation:

$$i = i_{\max} \frac{I}{I + I_s}, \quad (1)$$

where i is the response amplitude (pA), $i_{\max}$ is the maximum dark current (pA), measured as the amplitude of the response to a saturating flash (closing all light-sensitive channels), I is flash intensity (photons μm^{-2}) and I_s is half-saturating flash intensity. The half-saturating intensity is inversely proportional to *fractional sensitivity*, i.e. the fraction of the light-sensitive current that is turned off by one photoisomerization. Changes in $i_{\max}$ and I_s were followed throughout each experiment (for an example, see Fig. 2).

Determination of pigment composition: measurements of spectral sensitivity and spectral absorbance

Spectral sensitivity measurements. The spectral sensitivity of each cell was determined both in the native and the final state, i.e. before bleaching and after regeneration of the visual pigment with 11-*cis*-retinal. The half-saturating intensity at seven test wavelengths in the range 440–740 nm was determined relative to that at the reference wavelength 540 nm (λ_{ref}). A series of 5–15 dim-flash responses at each test wavelength was interleaved between complete intensity–response families recorded at 540 nm. The flash intensity at each test wavelength was selected to elicit *ca* 10–20% of the saturated response amplitude. Equation (1) was fitted to the intensity–amplitude data recorded at each test wavelength (λ) assuming that i_{max} was the same as in the immediately preceding full 540 nm intensity–response family, thus yielding the half-saturating intensity parameter $I_s(\lambda)$ for the test wavelength. Observing that fractional sensitivity is inversely proportional to $I_s(\lambda)$, the *relative fractional sensitivity*, $S(\lambda)$, at each test wavelength is

$$S(\lambda) = \frac{I_s(\lambda_{ref})}{I_s(\lambda)}. \quad (2)$$

Microspectrophotometry (MSP). A single-beam microspectrophotometer (MacNichol, 1978) was used to record visual pigment absorbance spectra from rod outer segments under dark-adapted conditions and following bleaching and regeneration of visual pigment. Spectra for the native state were recorded in rods taken from the same cell suspension as used for electrophysiological recordings. In each experiment, 10 intact rods or isolated outer segments containing the native visual pigment were studied. Another set of absorbance spectra were recorded after total bleaching and regeneration of the visual pigment with 11-*cis*-retinal. The rods in these latter recordings, however, were from retinas different to those used for the electrophysiology, as it was not essential that the initial A2/A1 ratio was exactly the same as in any single electrophysiological experiment. For convenience we therefore chose to do the MSP regeneration measurements separately from electrophysiology experiments.

A small volume of cell suspension in Ringer solution (50 μl) was placed between two cover slips that were sealed together with double-sided tape. The optical density of rod outer segments was recorded over the wavelength range 380–740 nm. The rectangular measuring beam was aligned parallel to the long axis of the outer segment (OS), covering *ca* 1/4 of its width. The axis of polarization of the measuring light was orthogonal to the long axis of the OS. Before each scan, a baseline recording was measured in a cell-free space adjacent to the OS. Typically, 10 scans were averaged in each case. The mean optical density (O.D.) between 400 and 740 nm was calculated by the data acquisition software as O.D. $= \log(I_0/I_t)$, where I_0 is the incident light intensity measured in the cell-free space and I_t the transmitted light through the OS. The spectra were baseline-corrected by subtracting from each data point a value given by a straight line least-squares-fitted to the data points over the interval 650–700 nm, where the absorbance of the visual pigment is negligible (for further details, see Govardovskii *et al.* 2000).

Estimation of visual pigment composition. Spectral sensitivity and absorbance data were fitted with a sum of A1 and A2 visual pigment templates of Govardovskii *et al.* (2000). These templates are uniquely defined by a single variable (λ_{max}), whereby $\lambda_{max,A1}$ and $\lambda_{max,A2}$ are coupled according to the rule: $\lambda_{max,A2} = 1.575\lambda_{max,A1} - 263$ (nm) (Hárosi, 1994). Estimates of the molecular ratios of A1 and A2 pigments were deduced from the weights of the two templates in the sum that provided the best fit to normalized data as judged by a least-squares criterion in the wavelength range 440–700 nm. The fitting was performed on a linear sensitivity scale in the case of absorbance spectra recorded by MSP, where the range of reliable absorbance values covers less than 2 log units of absorbance. In the case of relative spectral sensitivity determined electrophysiologically the fitting was done on a log sensitivity scale (see Fig. 1). The reason is that the range of reliable spectral sensitivity values spans as much as *ca* 6 log units. Furthermore, the data points in the long-wavelength region having the lowest absolute sensitivity values depend strongly on differences in the A1/A2 pigment ratio. Thus, these points will be most efficiently taken into account, while fitting the spectral sensitivity data on a logarithmic scale. In the fitting routine, we assumed $\lambda_{max,A1} = 502$ nm (Makino *et al.* 1999), which provided an excellent fit to absorbance spectra recorded after a complete bleach and regeneration with A1 chromophore (see Fig. 1*B*). Furthermore, we assumed $\lambda_{max,A2} = 528$ nm as predicted by the Hárosi (1994) relation for $\lambda_{max,A1} = 502$ nm (see above). The ratio of peak photosensitivities of A1 and A2 pigments was taken to be 1.42 (Dartnall, 1968). Thus, our estimates of A1 and A2 percentages (see Table 1) refer directly to the relative numbers of A1 and A2 visual pigment molecules.

Single-photon response analysis

The membrane current response to isomerization of a single rhodopsin molecule (the single-quantum response, abbreviated SQR) was estimated by measuring the mean and the time-dependent ensemble variance of a sequence of dim-flash responses (see, e.g. Rieke, 2000). This method

assumes that the variability in response amplitude can be accounted for primarily by variability in the number of photoisomerizations Rh* per flash. For a Poisson distribution in Rh* per flash, the square of the mean response $\bar{r}^2(t)$ will be proportional to the ensemble variance of the response $\sigma_r^2(t)$ according to $\bar{r}^2(t) = \bar{n}\,\sigma_r^2(t)$, where the scalar $\bar{n}$ is the expected number of Rh* per flash and t is time. We estimated $\bar{n}$ by scaling $\sigma_r^2(t)$ to match $\bar{r}^2(t)$. The SQR size and waveform, $\hat{r}(t)$, can be estimated as: $\hat{r}(t) = \bar{r}(t)/\bar{n}$. This method does not take into account variation in the amplitudes of individual SQRs. In rods, the variance due to this is *ca* 20% of the SQR amplitude (Baylor *et al.* 1979*b*, 1984), which limits the accuracy of individual estimates obtained by this method.

Sequences of 30–50 dim-flash responses were recorded regularly throughout the experiment. We used two different flash intensities, nominally producing 2.1 and 4.3 Rh* on average. Each response was baseline-corrected to remove DC drift by subtracting from each data point of the response the ensemble average of the membrane current recorded over the initial 200 ms time window preceding response onset.

An independent estimate for SQR amplitude was based on photometric calibration of the stimulus light and measurement of the cell's collection area (A_c). The collection area was estimated by the following approximation (Baylor *et al.* 1979*b*; Cornwall *et al.* 2000):

$$A_c = \frac{(\ln 10)\pi d^2 l f \varepsilon \gamma}{4}, \qquad (3)$$

where d is OS diameter, l is OS length, ε is the specific optical density at the stimulus wavelength 540 nm ($\varepsilon = 0.0118\ \mu m^{-1}$, Cornwall *et al.* 2000), γ is the quantum efficiency for bleaching ($\gamma = 0.67$; Dartnall, 1972), and f is an 'orientation factor' = 0.5 for unpolarized light. Cell dimensions d and l were estimated from bright-field images of the cell. If the incident flash intensity based on photometric calibration is I, then $\bar{n} = A_c I$ and $\hat{r}(t) = \bar{r}(t)/\bar{n}$. The SQR amplitude estimated in this way for each individual dim flash sequence was generally within 20% of the estimates obtained from ensemble mean and variance.

We fitted dim-flash responses with a modified version of a function used by Schneeweis & Schnapf (2000) for macaque rods:

$$r(t) = (1 - w(t))r_1(t) + w(t)r_2(t), \qquad (4)$$

where $w(t) = (1 + (\tau_3/t)^m)^{-1}$, $r_1 = At^n \exp(-t/\tau_1)$, $r^2 = B(\exp(-t/\tau_2) - \exp(-t/\tau_3))$ and A and B are constants. This function has no mechanistic meaning and was used as a purely empirical equation for smoothing and zero-padding responses. Zero-padding implies that extra zero values are added after the end of the response (comprising in our case 10.23 s, 1024 points) to extend the full stretch used for analysis (in our case to 41 s, 4096 points). The purpose is to extend the spectral frequency range (see e.g. Vu *et al.* 1997) when power spectral densities are calculated as explained below. These model fits were also used to estimate the integration time of dim-flash responses (Baylor & Hodgkin, 1973):

$$t_i = \int_0^\infty \frac{r(t)}{r_{peak}} dt, \qquad (5)$$

where t_i is the integration time, $r(t)$ is the response (in our case eqn (4) fitted to the averaged SQR) and r_{peak} is the response amplitude (at peak).

Analysis of dark noise power spectra and the estimation of dark event rates per cell

The rate of 'dark' isomerizations per rod was estimated on the basis of power spectral densities of membrane current measured in darkness and in bright light. The analysis of power spectral densities has been widely used in earlier studies on dark event rates in both rod and cone photoreceptors (Lamb & Simon, 1977; Schwartz, 1977; Baylor *et al.* 1980; Bodoia & Detwiler, 1985; Leibrock *et al.* 1994; Rieke & Baylor, 1996, 2000; Schneeweis & Schnapf, 2000; Sampath & Baylor, 2002; Kefalov *et al.* 2003; Holcman & Korenbrot, 2005). One-sided power spectral densities of membrane current traces recorded in darkness, in bright light and in dim background light were calculated using the algorithms of the Clampfit 9.2 program (Axon Instruments), which rely on a fast Fourier transform of the input signals. Power spectra were determined from current sweeps each of which was 81.92 s in length. The total durations of recordings in each experiment in the native and final states were typically as follows: *ca* 30 min (complete darkness), *ca* 7 min (under each dim background light) and *ca* 20 min in bright light. Linear drift was first removed by subtraction of the best-fitting straight line from the data. Power spectral densities of current traces were then calculated over 40.96 s current segments with 50% overlap using cosine windowing. Power spectra of quantal events were calculated similarly using the zero-padded SQR (40.96 s) estimates obtained by fitting eqn (4) to the original SQRs (10.24 s) (see above). We estimated the instrumental Johnson noise level using the Nyquist equation: $S(f) = 4\,kT/R$, where k is the Boltzmann constant, T is the absolute temperature and R is the resistance of the pipette with the cell in place. In all of the studied cells the estimated instrumental noise level nicely matched the plateau level of the noise power spectral densities between *ca* 3 and 20 Hz (as an example, see the dashed line in Fig. 4*B*).

Noise not associated with the light-sensitive current of the rod was recorded after the strong bleaching exposure (see Fig. 2) and in bright (saturating) light at the end of the experiment. The noise due to discrete and continuous

membrane current fluctuations of the rod was then isolated as the difference between the power spectral densities measured in complete darkness minus the power spectral densities of noise measured in saturating light conditions. In order to separate continuous from discrete noise, the plateau of the difference spectra in the frequency range 0.3–0.5 Hz was fitted by a straight horizontal line representing the zero-frequency asymptote of the continuous noise component. The difference spectrum in the frequency range 0.018–0.21 Hz was then fitted with the sum of the continuous noise asymptote plus the SQR power spectrum multiplied by a scaling factor that gave the optimal fit (see Fig. 5). This factor expresses how many dark events of the given shape and size must occur within the duration of the recording on which the power spectrum is based to produce the dark current variance observed. Thus the event frequency per cell was obtained by dividing the scaling factor by the record duration (40.96 s) used for construction of each power spectrum. The method is identical to that of Kefalov *et al.* (2003), with the exception that we corrected for the contribution of the continuous noise component as mentioned above. The advantage of the analysis described above is that the goodness of the fit can be judged immediately from the match of the recorded low-frequency noise spectral densities and the theoretical spectrum (the sum of the scaled SQR power spectrum and the continuous noise plateau).

Estimation of dark event rates per molecule of visual pigment

Molecular rate constants (k) for spontaneous visual pigment activations were calculated as:

$$k = \frac{f}{P}, \tag{6}$$

where f is the mean frequency of dark events per cell estimated from the low-frequency component of the power difference spectrum and P is the total number of visual pigment molecules in the part of the outer segment 'seen' by the electrophysiological recording, estimated as $P = cV$. Here, c is the visual pigment concentration in the OS (3.27 mM in red rods of the larval salamander: Hárosi, 1975) and V the effective volume of the part of the OS outside the constriction of the suction pipette (see Table 1). We estimated V by measuring the OS diameter (d) and length outside the pipette (l) from bright-field images of the cell ($V = \pi d^2 l/4$).

Error estimates throughout are given as standard error of means (S.E.M.S) unless otherwise stated.

Estimating the total dark current variance and decomposing it into continuous and discrete noise components

The total dark noise variance arising from the phototransduction cascade was estimated by fitting the difference spectra (dark – bright light) by a linear combination of two functions, one representing continuous noise and the other discrete noise, and then integrating the fitted functions in the domain 0–20 Hz.

The discrete noise component was fitted by the scaled power spectrum of the SQR used for the analysis of dark event rates and obtained as explained above (eqn (4)). The continuous noise component in most cells was fitted with a function of the form:

$$S(f) = \frac{S(0)}{\left(1 + \left(\frac{2\pi f}{n\alpha}\right)^2\right)^n}, \tag{7}$$

where $S(0)$ is the zero-frequency asymptote of the continuous noise component, f is the frequency and n and α are model parameters (for further details, see Lamb & Simon, 1977; Baylor *et al.* 1979*b*). Equation (7) gives the power spectrum of a 'Poisson'-type impulse response, but it is used here strictly as a phenomenological description of the continuous noise spectrum (with $n = 5$, cf. Vu *et al.* 1997). However, in a few cells with even steeper high-frequency roll-off than given by eqn (7), a power function was fitted instead to the high-frequency edge (see Table 1 for results).

Results

Visual pigment content in the native state and after bleaching and regeneration

Pigment densities and the relative proportions of chromophores A1 and A2 were assessed by measuring the spectral properties of cells in the beginning (native state) and at the end (final state) of each experiment. The spectral sensitivity of the investigated rod was measured electrophysiologically in both states. For the native state, this was supplemented by MSP recordings of spectral absorbance in samples of rods from the same retina. Further, the general success of regeneration with the A1 chromophore after bleaching was assessed by MSP recording in samples of rods from other retinas. The pigment composition (A1 : A2 ratio) was determined by fitting the recorded spectra with sums of Govardovskii *et al.* (2000) templates for A1 and A2 visual pigments using a least-squares criterion (see Methods for further details).

Figure 1 shows spectra from one experiment. Red symbols and curves refer to the native state, blue symbols and curves to the final state after pigment bleaching and regeneration. In Fig. 1*A*, spectral sensitivities of the

rod (cell 3 in Table 1) are plotted on a logarithmic ordinate relative to the peak of the final-state (blue) spectrum, which has been normalized to unity (log relative sensitivity = 0). The fitted curves correspond to A1 : A2 = 30.0% : 70.0% in the native state and 90.4% : 9.6% in the final state. Figure 1*B* compares two MSP spectra, one representing the native state (averaged from 10 rods from the same retina as that in Fig. 1*A*), the other representing the final state after exposure to a light that was calculated to have bleached > 99% of the pigment and pigment regeneration with the A1 chromophore (averaged from 14 rods from a different retina). The fit to the native spectrum indicates an average A2 fraction of 81% in this rod sample, slightly higher than derived from spectral sensitivities for the single cell in Fig. 1*A*. The pigment spectrum following regeneration with the A1 chromophore after the nearly complete bleach is well-fitted by a pure A1 (502 nm) template (blue curve) with peak optical density 0.151, indicating satisfactory regeneration. The ratio of the peak absorbances of the two spectra is 1.426, consistent with strong A2 dominance in the native spectrum (cf. Dartnall, 1972).

In both panels *A* and *B* of Fig. 1, the native and final spectra cross near 540 nm, previously found to be the isosbestic point for A2 and A1 in salamander rod pigment (Cornwall *et al.* 2000). Light of this wavelength (that of the isosbestic point) will produce the same number of photoisomerizations in a rod regardless of the chromophore proportions, and it was therefore a convenient choice for stimulus wavelength in our experiments.

The mean values for the A1 : A2 ratio as estimated from spectral sensitivities in the five rods where complete experiments were achieved were 26% : 74% in the native state and 91% : 9% in the final state (see Table 1). The mean native-state estimate based on MSP spectra of rod samples from the same retinas was 20% : 80%. The presence of *ca* 10% A2 in the final state is consistent with the nominal 90% bleach (see Methods).

Time course of changes in light-sensitive current and fractional sensitivity before and following bleaching and regeneration

Figure 2 illustrates the time course of changes in light-sensitive current (saturating response amplitude) and fractional sensitivity that occurred before and following exhaustive bleaching of the native visual pigment and then during regeneration of visual pigment with the A1 chromophore.

Recordings such as are illustrated were successfully completed on five rods where the full experimental protocol lasted 10–14 h. These data were used for the further analysis. The characteristics of these cells, which had been selected for a high A2 content in the native state, are summarized in Table 1. The data illustrated are from cell 1 in Table 1. Figure 2*A* shows four examples of response families, recorded at the time points indicated by arrows in (Fig. 2*B*). The light-sensitive current and fractional

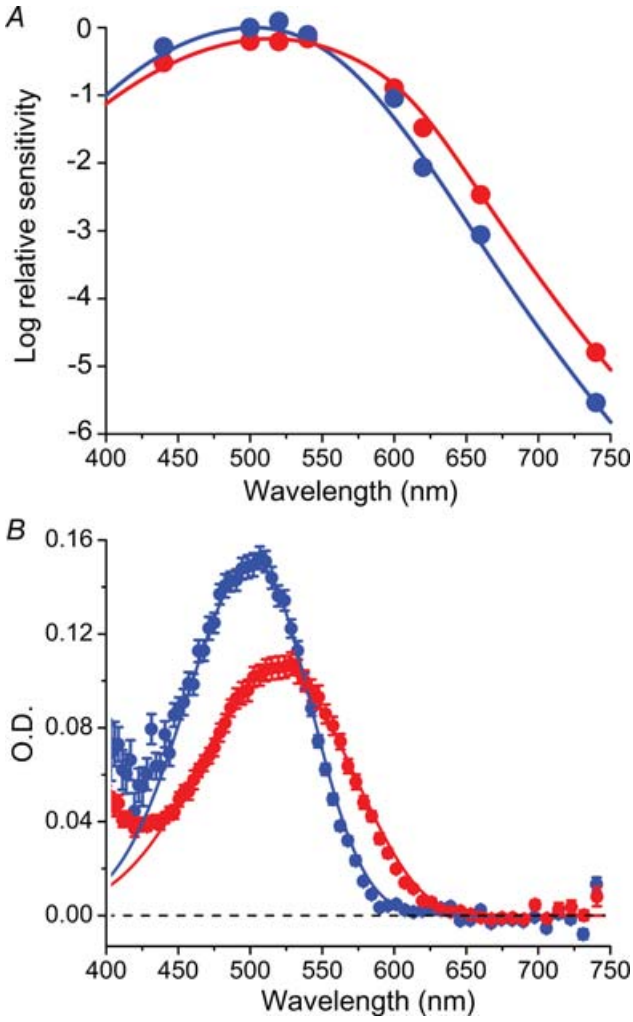

Figure 1. Determination of pigment content in rods before and after bleaching and regeneration with A1
A, log values of relative spectral sensitivities determined electrophysiologically in one rod (cell 3 in Table 1). Red, native state; blue, final state after *ca* 90% bleach and regeneration with A1. The curves fitted to the data are sums of Govardovskii *et al.* (2000) templates for A1 (λ_{max} = 502 nm) and A2 pigments (λ_{max} = 528 nm). In the native state, a fair fit (red curve) is obtained for a sum of templates corresponding to molecular proportions 30.0% A1 and 70.0% A2; in the final state (blue curve) the proportions are 90.4% A1 and 9.6% A2. The peak value of the 'final' spectrum has been normalized to unity and all sensitivities are expressed relative to this. The crossing point of curves lies at *ca* 546 nm and the ratio of the peak values (final/native) is 1.46. *B*, absorbance spectra recorded by MSP. The ordinate gives optical densities (O.D.) at each wavelength. Red: native state, mean ± S.E.M. of 10 rods from the same retina as the cell in *A*. Blue: final state, means ± S.E.M. of a sample of 14 cells from a different retina after a complete pigment bleach and regeneration with A1. The red curve is a sum of Govardovskii *et al.* (2000) templates for A1 and A2 corresponding to molecular proportions 19% A1 and 81% A2. The blue curve is a pure A1 (λ_{max} = 502 nm) template. The crossing point lies at *ca* 539 nm and the ratio of the peak O.D. values (A1/native) is 1.43. Error bars show S.E.M.

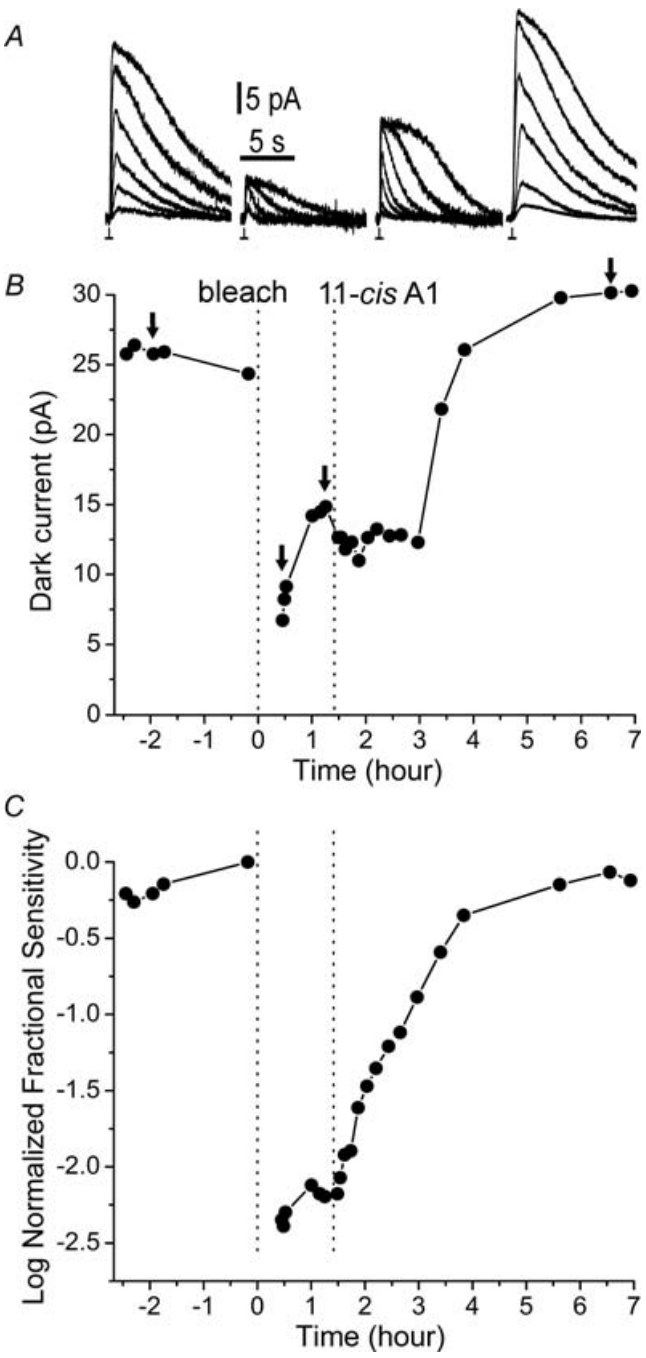

Figure 2. The time course of changes in the light-sensitive current and fractional sensitivity of one rod throughout a complete experiment

The vertical dashed lines mark the time points of: (1) the bleaching exposure ($t = 0$ min, middle point of 30 s light exposure); (2) introduction of *ca* 40 μM 11-*cis*-retinal ($t = 89$ min). Bath perfusion was halted for 20 min after the addition of 11-*cis*-retinal to incubate cells in the Ringer solution containing 11-*cis*-retinal. *A*, response families recorded at the times indicated by arrows in *B*. Flashes were 540 nm, 20 ms square-wave pulses. Each trace is the average of 1–30 responses to the same nominal flash intensity; intensities (photons μm^{-2} $flash^{-1}$) increased in 0.5 log unit steps starting at the following values (response families from left to right, n = number of flashes averaged): 0.242 ($n = 5$); 271 ($n = 1$; the intensity step from the first to the second response was 1 log unit in this case to avoid crowding); 23.0 ($n = 5$); 0.242 ($n = 20$). The light-sensitive current and fractional sensitivity values plotted in *B* and *C* were determined by fitting Michaelis functions to flash intensity–response amplitude data of this type recorded throughout the experiment (see Methods). *B*, time course of changes in the light-sensitive current. *C*, time course of changes in log fractional sensitivity. Fractional sensitivity values have been normalized relative to the peak value. (Cell 1 in Table 1.)

sensitivity, plotted in panels *B* and *C*, were determined by fitting Michaelis functions (eqn (1) in Methods) to flash intensity–response amplitude data extracted from response families such as those shown in Fig. 2*A*. Note that the maximum light-sensitive current (i_{max}) and the half-saturating flash intensity (I_S) (proportional to fractional sensitivity) are independent parameters in eqn (1), and although both change strongly after a bleach and during regeneration, the changes can be followed independently. Thus, panels *B* and *C* in Fig. 2 trace two independent processes (i.e. in fractional sensitivity, changes in i_{max} have been factored out).

In the native dark-adapted state (from −2.5 h to time = 0 in Fig. 2*B* and *C*), the light-sensitive current in this cell was *ca* 25 pA. At the end of the experiment, following regeneration, the current had reached *ca* 30 pA, suggesting that there had been no general physiological deterioration over the course of the intervening measurements. At time 0 (first vertical dashed line), the cell was exposed to a 30 s bleaching light calculated to have bleached *ca* 90% of the pigment. This light exposure resulted in complete suppression of the current for *ca* 20 min. Following this initial phase, the current recovered back to a level that was about 60% of the original dark current. This partial recovery was interrupted and even slightly reversed by the application of 40 μM 11-*cis*-retinal in the bath (second vertical dashed line at 85 min = 1.4 h), as has been previously reported (Kefalov *et al.* 2001). Further recovery was delayed for almost 100 min (1.7 h) in this experiment, and in no experiment for less than 60 min. The plateau phase was followed by a final exponential return of the light-sensitive current, which was complete in 4–5 h after the introduction of the 11-*cis* chromophore. The major difference in the recovery of fractional sensitivity (Fig. 2*B*) compared with the light-sensitive current is that the introduction of the chromophore immediately triggered a monotonic rise that could be described by a single exponential (time constant *ca* 90 min for the cell in Fig. 2) all the way to the final dark-adapted state.

These data are qualitatively consistent with those of Cornwall *et al.* (2000), who found that no response could be elicited immediately after bleaching 50–75% of the pigment, that the new steady state of the dark current (40% of the initial dark current) was reached within 50 min after the bleach, and that the recovery

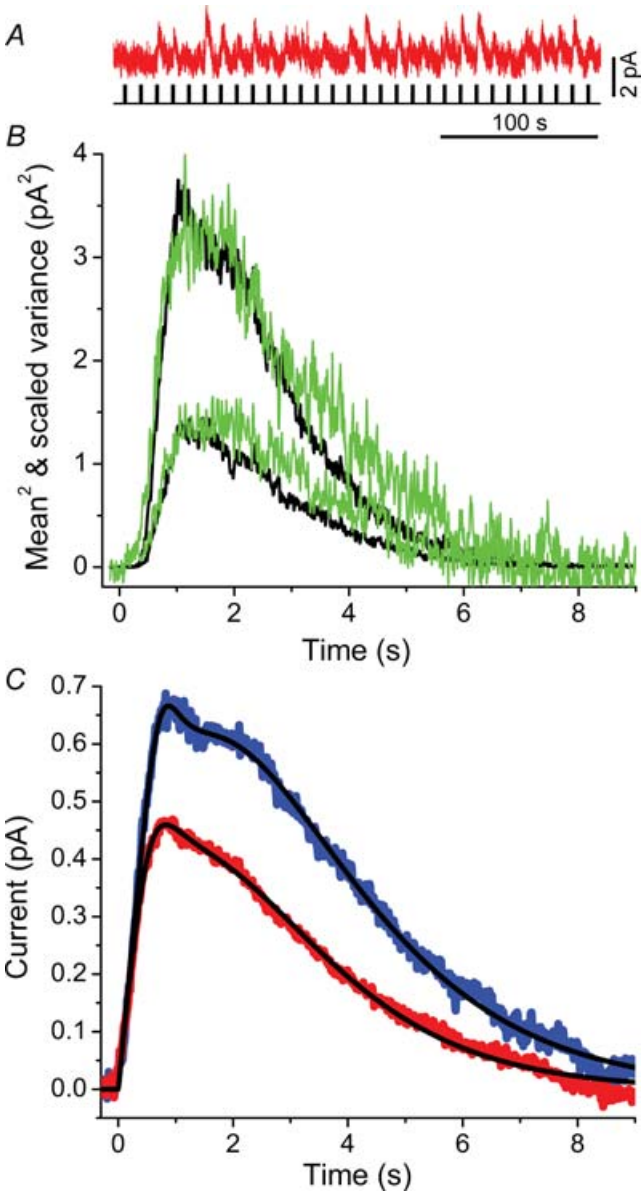

Figure 3. The single-photon response
A, response variation exemplified in a sequence of 30 responses to the same nominal flash intensity (2.0 Rh* flash^{-1}; $A_c = 19\ \mu m^2$) in the native state. Cell 4 in Table 1. *B*, square of the mean response (black) and scaled time-dependent ensemble variance (green) of dim flash responses at two different nominal light intensities (2.0 Rh* flash^{-1}; $A_c = 19\ \mu m^2$) and (4.1 Rh* flash^{-1}; $A_c = 19\ \mu m^2$) in the native state, same cell as in *A*. At both light intensities the results are based on three separate sequences of 30 responses each. The scaling factor of variance provides an estimate of the mean number of photoisomerizations produced by the flash: 4.0 Rh* at the higher intensity (cf. nominal value 4.1) and 2.6 Rh* at the lower intensity (cf. nominal value 2.0). The estimates for single-quantum amplitude are obtained simply by dividing the mean response by the scaling factor of the variance. The estimates for single quantum response (SQR) amplitude derived from the two examples in the figure are 0.50 pA (based on the responses to the brighter flash light intensity) and 0.47 pA (based on the responses to the lower flash intensity). *C*, the mean SQR in the native state (red) and the final state (blue); same cell as in *A* and *B*. The responses are averages of 7 SQR estimates obtained at different times of the experiment from the same cell. Each of these seven individual SQR estimates used for the calculation of the mean SQR were obtained by comparison of the squared mean response and the variance of a sequence of responses to 30–50 dim flashes such as shown in *A*. By estimating the SQR size at different times throughout the experiment, we could also check whether any systematic changes in the SQR amplitude occurred during the experiment. The black curves are model fits according to eqn (4).

of sensitivity upon the addition of 11-*cis*-retinal (5 μM) took *ca* 2 h. It should be noted, however, that the recovery time courses after bleaches depend critically on the experimental protocol. Kefalov *et al.* (2001) found significantly faster recovery than either Cornwall *et al.* (2000) or the present study, which is probably due to the following three main differences in the experimental parameters. (1) Kefalov *et al.* (2001) used lipid vesicles and a high concentration (100 μM) of 11-*cis*-retinal for regeneration. This gives significantly faster kinetics of recovery: in our own control experiments both dark current and fractional sensitivity recovered more than 2 times faster when 11-*cis*-retinal was added in lipid vesicles (180 μM) than when ethanol solution (40 μM) was used in otherwise similar experimental protocols, including in both cases 20 min exposure of the cell to the retinoid solution. (The rates of recovery were measured by the times needed for 70% recovery upon addition of 11-*cis*-retinal.) (2) Kefalov *et al.* (2001) used 20% bleaches compared with 50–75% in Cornwall *et al.* (2000) and 90% here. Stronger bleaches will suppress the dark current for longer times, as demonstrated in salamander red rods by Tsina *et al.* (2004). (3) The duration of the plateau phase where no dark current recovery occurs (although sensitivity does recover) may vary with the time of incubation in 11-*cis*-retinal. The plateau might be related to the non-covalent interaction between 11-*cis*-retinal and opsin (Kefalov *et al.* 2001), which would be relieved only when the exogenous retinoid is washed out. Our retinoid exposure (20 min) was much longer than that of Kefalov and colleagues. However, the exact mechanisms and time courses of the recovery of dark current and fractional sensitivity are beyond the scope of this study.

The noise analyses and SQR determinations (see Figs 3–5 below) are based on measurements made during epochs of darkness and dim backgrounds as well as dim-flash responses recorded in the longer intervals where panels *B* and *C* show no data points (see, for instance Fig. 2, *ca* 1.5 h before the bleach and then during the last 2.5 h of the experiment, when sensitivity had essentially recovered). Instrumental noise was recorded during the post-bleach period when the light-sensitive current was zero and again at the end of each experiment in continuous bright light that closed all the light-sensitive channels.

The quantal response

The size and shape of the SQR was determined by analysing response variance in sequences of 30–50 presentations of dim flashes at two different intensities nominally delivering 2.0 and 4.1 Rh* (see Methods). In Fig. 3*A*, the trace shows one recording sequence including 30 flashes (nominal intensity 2.0 Rh*; the recording is from cell 4 in Table 1). It is possible to discern variation in response amplitude as well as response failures. If the variation is due to Poisson variation in the actual numbers of photoisomerizations produced on successive presentations of the same nominal flash intensity, the time-dependent ensemble variance should have the same waveform as the square of the mean response and the scaling factor required to make the traces coincide is then equal to the mean number of photoisomerizations per flash actually delivered in the series (see Methods). Figure 3*B* shows a comparison of variance (green traces) and mean squared (black traces) for response series to two nominal flash intensities, each comprising 90 presentations (i.e. 3 similar series as shown in panel *A*). The traces with smaller amplitude are based on responses to nominal flash intensity 2.0 Rh* (including the series shown in panel *A*), the traces with higher amplitude on responses to nominal flash intensity 4.1 Rh*. The waveforms show a satisfactory agreement. The scaling factors used to produce the best coincidence were 4.0 for the larger responses and 2.6 for the smaller responses. The SQR amplitudes (obtained by dividing the mean response by the scaling factor at both light intensities) were in both cases in the range 0.4–0.5 pA. Similar response series comprising 30–50 trials were recorded at different times during the experiments in order to study possible systematic changes in response amplitude. No significant changes were found.

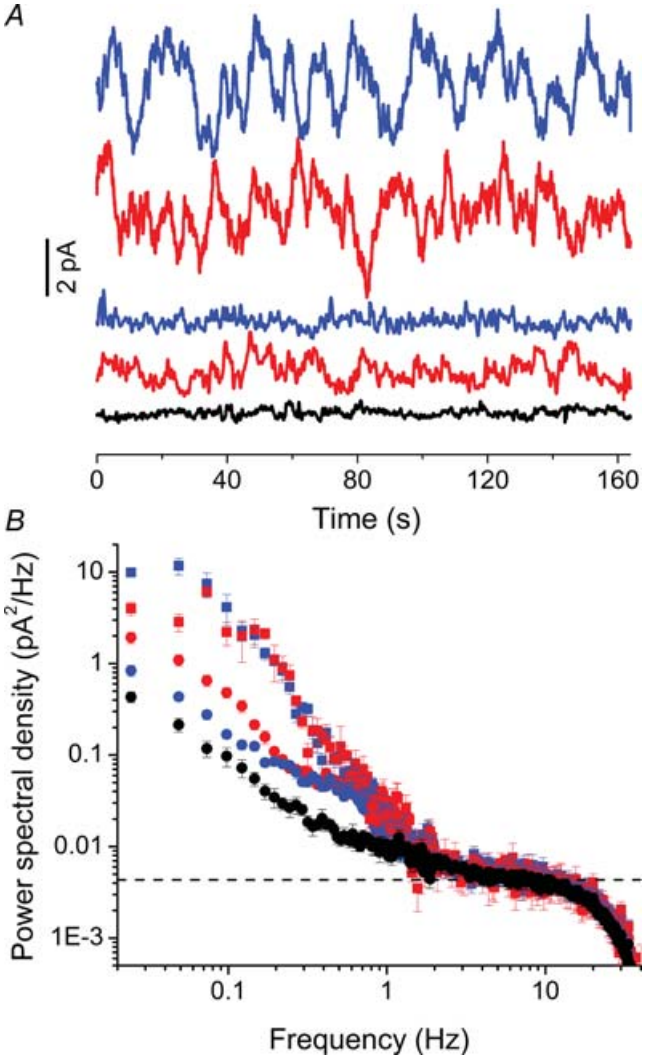

Figure 4. Noise recordings and power spectra
A, representative noise recordings. The two top traces show noise under a dim steady background light (2.4 Rh* s^{-1}) in the final (blue) and native (red) state; the two middle traces show dark noise in the final (blue) and native (red) state; the bottom trace shows instrumental noise (black). All traces have been low pass filtered at 1 Hz. Same cell as in Fig. 3. *B*, total noise power spectra based on many recording sequences similar to those shown in *A*. Spectra from top to bottom (according to the zero-frequency asymptote): blue squares, noise under the dim background in the final state; red squares, noise under the dim background in the native state; red circles, dark noise in the native state; blue circles, dark noise in the final state; black circles, instrumental noise. Power spectra were smoothed at higher frequencies by averaging over 5 neighbouring points in the frequency range 2–10 Hz and over 10 points in the frequency range 10–40 Hz. The dashed line shows the Johnson noise level (0.0043 pA^2 Hz^{-1}) calculated from the resistance with the cell in the pipette (3.8 MΩ).

Figure 3*C* shows the SQRs in the native state (red) and in the final state (blue) of the same cell as in Fig. 3*A* and *B*. Each was obtained by averaging responses obtained from seven sequences of 30 flash presentations such as shown in Fig. 3*A*, and scaling the amplitude of the averaged response by the numbers of photoisomerizations actually produced, estimated as exemplified in Fig. 3*B*. The SQR waveform could not be well described by filter models with a single basic time parameter, as often used for linear-range responses in rods or cones (e.g. Poisson or independent activation models as defined by Baylor *et al.* 1974, 1979*a*). Moreover, the waveform varied somewhat between cells and changed with the state of adaptation. Thus the kinetics of the response could not be meaningfully captured by one simple measure, such as the time to peak. We chose to express it in terms of integration time (t_i), defined as the integral of the response divided by its peak amplitude (eqn (5) in Methods).

In Fig. 3*C*, the SQR recorded in the final (A1) state was both larger and slightly more protracted than in the native (A2) state. This was true of three cells, whereas in two of the cells there was no significant difference in native and final SQR (Table 1). The smooth curves fitted to the responses in Fig. 3*C* are phenomenological descriptions according to eqn (4). The mean (±S.E.M.) values are: amplitude, 0.41 ± 0.03 pA (native) and 0.57 ± 0.07 pA (final); integration time, 3.16 ± 0.15 s (native) and

3.47 ± 0.26 s (final). If it is accepted that responses initiated by A1 and A2 pigment molecules in a single rod in a single state are indistinguishable, as has been shown to be the case in bullfrog (Firsov *et al.* 1994), differences in SQR reflect differences in the state of the cell's transduction machinery. One interesting possibility is that dark events occurring at a rate of about one per integration time in the native state could 'light-adapt' the rod causing a smaller and shorter SQR (see Discussion). Alternatively, the difference could be due to a general slowing-down of the response shut-off mechanisms over the course of the long experiment, causing a larger and longer SQR in the final state.

Dark noise and photon noise

Figure 4*A* shows representative samples of membrane current noise recorded under five different conditions, each comprising 164 s. Figure 4*B* shows noise power spectra corresponding to each of these conditions (but based on much longer recordings). The data are from the same cell as in Fig. 3. The traces in Fig. 4*A* show (from top to bottom): (i) noise under a dim (2.4 $Rh^* s^{-1}$) background light, recorded in the final state (blue trace); (ii) noise under the same background light recorded in the native state (red trace); (iii) dark noise recorded in the final state (blue trace); (iv) dark noise recorded in the native state (red trace); (v) instrumental noise recorded when the light-sensitive current had been abolished (black trace). The corresponding power spectra in panel *B* have been computed from a large number of noise epochs similar to those shown in panel *A*. For example, the data sets underlying the native- and final-state dark noise spectra in Fig. 4*B* comprise a total of 22 min recordings each and those under background light a total of 4 min of recordings each. Power spectral densities were calculated over 41 s segments from 82 s traces with 50% overlap (see Table 1 and Methods). The colour code of the spectra in Fig. 4*B* corresponds to that of the noise samples in Fig. 4*A*. 'Background' noise spectral densities are identified by squares and 'dark' noise spectral densities by circles.

It is immediately obvious from Fig. 4 that dark noise power at low frequencies is higher in the native (A2) than in the final (A1) state. By contrast, under a background light where photon fluctuations are strong enough to dominate over the random occurrence of thermal events, low-frequency dark noise is similar in the two states. At the two lowest frequencies (the two leftmost pairs of data points) there is a discrepancy between the two, evidently due to the limited recording time under background light (only 4 min in this cell), making the data susceptible to low-frequency artefacts. The 'background' power spectra cannot be perfectly fitted by scaling the power spectrum of the dark-adapted SQR, since the 2.4 $Rh^* s^{-1}$ background used light-adapts the cell, making the SQR smaller and faster. In the frequency domain, this corresponds to lowering the zero-frequency asymptote (S_0) and extending the power spectrum towards higher frequencies. These phenomena have been analysed for native salamander rods by Jones (1998), who predicts that the total discrete noise variance arising from a background light delivering 2.3 $Rh^* s^{-1}$ (i.e. practically the same as used here; the corresponding power spectrum is shown in Fig. 7 of Jones, 1998) is about 1.6-fold lower than would arise from the same rate of events having the amplitude and time course of the dark-adapted SQR (eqn (2) in Jones, 1998).

The instrumental noise (shown by black circles in Fig. 4*B*), on the other hand, has much less power in the low-frequency range than the dark noise of the rod. The 'biological' noise components that interest us here are those that are not present in the instrumental noise.

Figure 5 shows difference spectra isolating these biological components of the dark noise by subtraction of the instrumental noise (red, native state; blue, final state). The low-frequency branch of the difference spectra can be fairly well fitted by appropriately scaling the

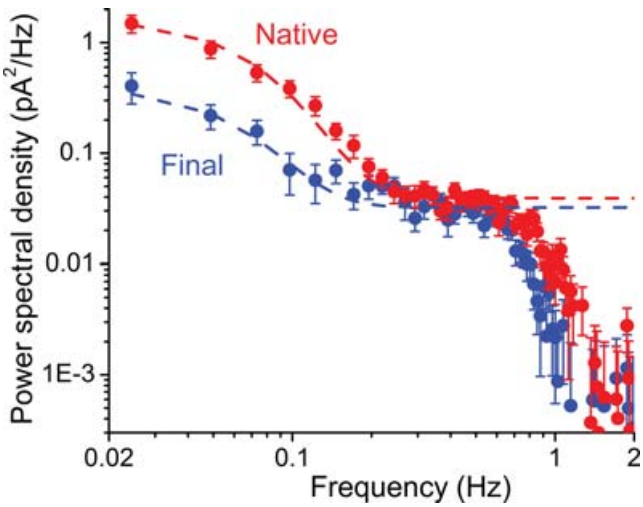

Figure 5. Difference spectra: dark noise – instrumental noise
Dark noise difference spectra calculated from Fig. 4. The instrumental noise has been subtracted from the total dark noise: red circles, native state; blue circles, final state. The low-frequency noise component has been fitted with the sum of the power spectrum of the continuous noise plateau level (averaged over 0.3–0.5 Hz) and the scaled power spectrum of the respective SQR, calculated from the responses shown in Fig. 3*C* (see Methods). These fitted curves are shown by dashed lines: red, native state; blue, final state. The difference in this component representing discrete noise indicates a *ca* 10-fold difference in dark event rate between the native and final states. (Note that the corresponding noise power in the final state is relatively increased by the larger SQR.) The continuous noise component has been fitted with a straight line in the plateau region. There is no significant difference in this component between the native and the final state.

Table 1. Summary of the main results from the five rods on which complete experiments were achieved

Cell	State	A1 (%)	A2 (%)	i_{max} (pA)	SQR (pA)	t_i (s)	σ^2_{dark} (pA^2)	σ^2_D (pA^2)	σ^2_c (pA^2)	Event freq. (Rh* s^{-1})	Rod OS vol. (μm^3)	Molecular rate constant (10^{-11} Rh* molecule^{-1} s^{-1})
1	Native	18.3 (17.0)	81.7 (83.0)	25.1	0.32	3.15	0.030	0.025	0.005	0.163	1810	4.59
	Final	94.3	5.7	30.1	0.53	3.64	0.008	0.005	0.004	0.0154		0.433
2	Native	22.3 (13.9)	77.7 (86.1)	34.7	0.38	2.96	0.048	0.034	0.014	0.318	2190	7.36
	Final	87.4	12.6	32.2	0.37	2.96	0.033	0.007	0.025	0.0519		1.20
3	Native	30.0 (18.8)	70.0 (81.2)	34.6	0.41	3.31	0.081	0.057	0.024	0.204	2040	5.08
	Final	90.4	9.6	37.8	0.78	3.66	0.063	0.037	0.023	0.0314		0.782
4	Native	31.0 (21.7)	69.0 (78.3)	48.0	0.46	3.62	0.141	0.105	0.036	0.244	1970	6.29
	Final	92.3	7.7	48.8	0.67	4.26	0.050	0.021	0.026	0.0183		0.472
5	Native	30.1 (27.9)	69.9 (72.1)	44.6	0.47	2.76	0.074	0.053	0.022	0.258	2550	5.15
	Final	88.9	11.1	40.8	0.51	2.81	0.019	0.010	0.008	0.0322		0.641
Mean ± S.E.M.												
	Native	26.3 ± 2.6 (19.9 ± 2.4)	73.7 ± 2.6 (80.1 ± 2.4)	37.4 ± 4.1	0.41 ± 0.03	3.16 ± 0.15	0.075 ± 0.019	0.055 ± 0.014	0.020 ± 0.005	0.238 ± 0.026	2110 ± 280	5.694 ± 0.501
	Final	90.7 ± 1.2	9.3 ± 1.2	37.9 ± 3.3	0.57 ± 0.07	3.47 ± 0.26	0.035 ± 0.010	0.016 ± 0.006	0.017 ± 0.005	0.030 ± 0.006		0.706 ± 0.138

Pigment composition (percentage A1 and A2), maximum current (i_{max}), the single quantum response (SQR) amplitude and integration time (t_i), total variance of dark noise (σ^2_{dark}), its discrete (σ^2_D) and continuous components (σ^2_c) as well as the estimates for the spontaneous event rates per cell and per molecule of visual pigment are given. The primary estimates for pigment composition were obtained from electrophysiological measurements of spectral sensitivity in the same cell (see Methods). For the native state, these were supplemented by MSP measurements on 10 cells obtained from the same cell suspension as that used in the experiment. The estimate of pigment composition obtained from these absorbance measurements are given in parentheses.

power spectrum of the respective SQR (responses shown in Fig. 3*B*). This suggests that it originates in such quantal events. The rate of these events that would account for the observed variance can be calculated from the fit. The dashed curves in Fig. 5 correspond to the best-fitting function obtained as a sum of the scaled SQR power spectrum and the plateau level of the remaining noise component, read approximately over the range 0.3–0.5 Hz (see Methods). In Fig. 5, the difference in the low-frequency branch between the native and final states can be explained by a *ca* 10-fold difference in dark event rates. (Note that for a given event rate, the noise power in the final (A1) state is relatively higher due to the larger SQR.) In the remaining noise component, the 'continuous' noise, there is no significant difference between the native and the final state, as is evident from the approximate coincidence of the spectra beyond *ca* 0.3 Hz in Fig. 5. The dark current variance associated with the two noise components was calculated by integrating the two theoretical curves fitted to the difference spectrum (dark – bright light) separately over the range 0–20 Hz (see Methods). The estimates for the variance arising from discrete events were 0.055 ± 0.014 pA^2 in the native state and 0.016 ± 0.006 pA^2 in the final state (mean ± S.E.M., see Table 1). By contrast, the variance estimates for the continuous noise component did not differ significantly between the two states, being 0.020 ± 0.005 pA^2 (native) and 0.017 ± 0.005 pA^2 (final). Thus, in the native state 73% of the total dark-current variance was associated with the discrete component, whereas in the final state both noise components contributed equally. The noise characteristics of the individual cells are given in Table 1.

Rates of thermal activation of A2 and A1 pigment molecules

The mean estimates for dark event rates in the native and final states are 0.238 ± 0.026 and 0.030 ± 0.006 Rh* s^{-1}, respectively. The underlying change in pigment composition entailed a decrease in the mean fraction of A2 pigment from $73.7 \pm 2.6\%$ (native) to $9.3 \pm 1.2\%$ (final). Thus the dark event rate decreased by $0.238/0.030 = 7.93$-fold as the A2 fraction decreased by

73.7/9.3 = 7.92-fold. To a first approximation the event rate appears to be directly proportional to the amount of A2 pigment, which thus would seem to dominate the generation of spontaneous events even in the final state.

The relation between event rate and A2 fraction can be extrapolated to 100% and 0% to provide estimates for the event rates of pure A2 and pure A1 pigment, respectively. Assuming (1) response univariance, i.e. that SQRs initiated in A1 and A2 pigment molecules under the same conditions are identical (Firsov *et al.* 1994), and (2) complete pigment regeneration, i.e. that the total number of functional pigment molecules in the cell is the same in the native and final states, event rates per rod (f) can be expressed as follows:

$$\begin{aligned} f_{\mathrm{A1}} &= k_1 x_{\mathrm{A1}} = k_1(1 - x_{\mathrm{A2}}) \\ f_{\mathrm{A2}} &= k_2 x_{\mathrm{A2}} \\ f_{\mathrm{total}} &= f_{\mathrm{A1}} + f_{\mathrm{A2}} = k_1 + (k_2 - k_1)x_{\mathrm{A2}}, \end{aligned} \qquad (8)$$

where f_{A1} and f_{A2} are the event rates per rod due to A1 and A2 pigment fractions (x_{A1}, x_{A2}). The measured event rate (f_{total}) is the sum of f_{A1} and f_{A2}, and k_1 and k_2 are constants. It can be seen from eqn (8) that the constants k_1 and k_2 correspond to the event rates of pure A1 and A2 pigment, respectively: at $x_{\mathrm{A2}} = 0, f_{\mathrm{total}} = k_1$(100% A1) and at $x_{\mathrm{A2}} = 1, f_{\mathrm{total}} = k_2$(100% A2).

We plotted f_{total} for each cell as a function of the A2 pigment content (corrected for volume differences) and fitted the data by linear regression according to eqn (8). The data and linear regression line are shown in Fig. 6 on both linear (Fig. 6*A*) and logarithmic (Fig. 6*B*) coordinates. Each cell is represented by two data points, one for the native and one for the final state. The advantage of the logarithmic plot (Fig. 6*B*) is that it expands the scales at small values of the variables, revealing a clear correlation between event rates and the small fractions of A2 remaining in the final state after bleaching and regeneration with A1 (lower left-hand group of data points). In the linear plot (Fig. 6*A*), the final-state data points are crowded near the origin and the correlation cannot be resolved.

To estimate the event rates for pure A2 and pure A1 pigment, we extrapolated the regression line to 100% and 0% A2 ($x_{\mathrm{A2}} = 1$ and 0, respectively). (Alternatively, we could have determined the constants k_1 and k_2: see above.) Thus, the estimate for f_{A2} is 0.324 ± 0.030 Rh* s^{-1}; that for f_{A1} is 0.0009 ± 0.0033 Rh* s^{-1}. (The estimation was done on linear coordinates, where it is possible to extrapolate to $x_{\mathrm{A2}} = 0$.) The S.E.M. values are based on the standard deviation of estimates obtained in this way from each cell separately. The relatively large S.E.M. for A1 reflects the fact that we have no measurements for very small A2 fractions (< 6%), and the estimate is sensitive even to small changes in the slope of the fitted line. Recalculated to event rates per molecule (denoted f_{mol}) using cell volume and estimated pigment concentration (see Methods), the estimates are $f_{\mathrm{mol,A2}} = (7.66 \pm 0.71) \times 10^{-11}$ Rh* molecule^{-1} s^{-1} and $f_{\mathrm{mol,A1}} = (2.1 \pm 7.8) \times 10^{-13}$ Rh* molecule^{-1} s^{-1}, respectively. The ratio of the means is 365, but obviously the error limits are wide. We calculated a lower-limit estimate for the factor by which A2 and A1 pigments differ in stability in two different ways: (1) by calculating in the linear domain the *lower* 95% confidence limit for $f_{\mathrm{mol,A2}}$ and the *upper* 95% confidence limit for $f_{\mathrm{mol,A1}}$; (2) by calculating in the logarithmic domain the lower 95% confidence limit for the ratio of the

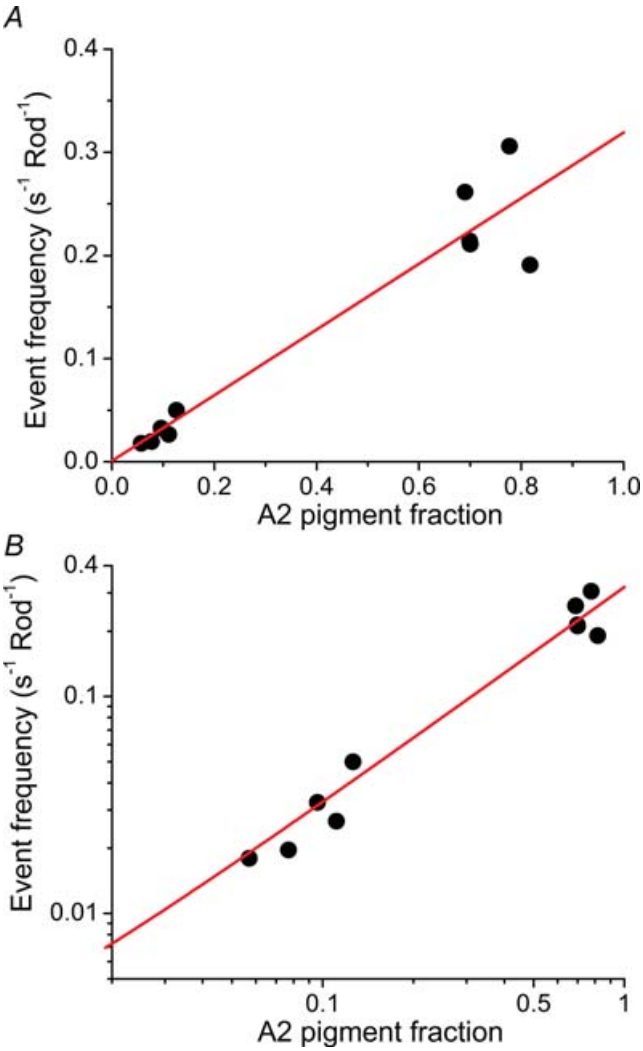

Figure 6. Dark event rates per rod as a function of the fraction of A2 pigment

A, the estimates of dark event rates of all 5 rods in Table 1 in the native and final states plotted against the fraction of A2 pigment. The red line shows the linear regression of event rate (y) on A2 content (x): $y = 0.0009 + 0.318x$. All event rates have here been normalized to the mean outer segment (OS) volume recorded in our experiments (2100 μm^3), thus correcting for volume differences in the individual recordings. *B*, the same data as in *A* shown on logarithmic scales.

geometric means ($f_{\mathrm{mol,A2}}/f_{\mathrm{mol,A1}}$). The two calculations give essentially consistent results:

(1) The 90% confidence limits of the (linear) estimates are mean $\pm$ 2.132 S.E.M. (Student's t distribution, d.f. = 4). Thus there is a one-tailed probability $P < 0.05$ for $f_{\mathrm{mol,A2}}$ to be smaller than 6.15×10^{-11} Rh* molecule^{-1} s^{-1} or for $f_{\mathrm{mol,A1}}$ to be larger than 0.19×10^{-11} Rh* molecule^{-1} s^{-1}. The ratio of these, 6.15/0.19 = 32, represents a lower limit for the ratio $f_{\mathrm{mol,A2}}/f_{\mathrm{mol,A1}}$ at the confidence level $P < (0.05 \times 0.05 =) 0.0025$.

(2) The log-transformed data allow statistical comparisons between the ratios of the mean estimates: the difference of means in the log-domain equals the logarithm of their ratio: $\log f_{\mathrm{mol,A2}} - \log f_{\mathrm{mol,A1}} = \log(f_{\mathrm{mol,A2}}/f_{\mathrm{mol,A1}})$. We calculated 95% confidence limits for the difference of logarithms (Student's t distribution) and then converted these limits back to the linear domain. The lower-limit estimate for the ratio of the geometric means thus obtained is 36, i.e. at the confidence level $P < 0.05$ the event rate of A2 pigment is at least 36-fold higher than that of the A1 pigment.

Discussion

Steady-state dark noise has here been measured for the first time in the same rod before and after bleaching most of the visual pigment and regenerating with a different chromophore. This made it possible to study the effect of the A2 $\rightarrow$ A1 switch, while avoiding possible differences in several other factors, notably in the opsin and other transduction proteins. The results are discussed in relation to earlier work on dark noise in photoreceptor cells and the thermal stability of visual pigments differing with respect to chromophore and spectral sensitivity.

Comparison with earlier studies on salamander rods in the native state

The power spectra of dark noise measured in native rods were qualitatively similar to those measured earlier in red rods of the same and other vertebrate species. Spectra could be construed as the sum of a low-frequency component, attributed to spontaneous activation of the visual pigment, and a component extending to somewhat higher frequencies, attributed to spontaneous activation of phosphodiesterase (PDE) (Baylor *et al.* 1980, 1984; Rieke & Baylor, 1996). The cut-off frequencies of these noise components (i.e. the frequencies where noise power has dropped by 50% from the maximum given by the zero-frequency asymptote, *ca* 0.1 and 1 Hz, respectively) as well as their relative contributions to total dark current variance were similar to values reported earlier for salamander rods (Vu *et al.* 1997; Jones, 1998). We attribute 73% of the dark variance to the discrete component, where Vu *et al.* (1997) give 67% and Jones (1998) 62%. Since these earlier studies do not give the A1 : A2 ratios of the rods, such minor differences may be due to differences in the A2 pigment content. We specifically selected a batch of salamanders with a high A2 fraction for our experiments.

By contrast, the dark event rate reported by Vu *et al.* (1997), 0.030 ± 0.005 Rh* s^{-1}, is significantly lower than our estimate for native rods (0.238 ± 0.026 Rh* s^{-1}) and close to the value we find for rods with *ca* 90% A1 pigment (0.030 ± 0.006 Rh* s^{-1}). In view of the similarity of the noise power spectra in our study and theirs, this difference must arise in the analysis. Vu *et al.* (1997) based their estimate on visual counting of discrete events in matched-filtered records of dark current. In rods with distinct quantal bumps (e.g. toad), this method does give results consistent with those based on power spectrum analysis (Baylor *et al.* 1980). However, we have found that the method is unreliable in salamander rods with their relatively small SQRs and significantly higher event frequency as compared with e.g. toad rods. The method relying on dark noise power spectra is superior to alternative methods when the SQR amplitude is small and the frequency of events high, as is the case especially in native salamander rods compared with e.g. toad rods (Baylor *et al.* 1980). We re-analysed the dark noise power spectra of Vu *et al.* (1997; their Figs 1–3) based on their own data: asymptote of the discrete noise component $S_0 = 0.35$ pA^2 Hz^{-1}; SQR amplitude *ca* 0.7 pA, response waveform according to their model. Our analysis suggests that the dark event rate in their rods was roughly 0.16 Rh* s^{-1}. Although somewhat lower than the estimates for our native-state rods, this value would be our prediction for a 50 : 50 ratio of A1 : A2 (see Fig. 6), which according to our experience is not unusual in larval salamanders.

The effect of the chromophore switch on dark noise

The chromophore switch (A2 $\rightarrow$ A1) was associated with a significant drop in dark noise power at the low frequencies where the scaled power spectrum of the SQR provided a good fit, whereas the 'continuous' noise component showed no systematic change. The latter observation is not surprising, as the effect of pigment dark activity on the average number of PDE molecules available for spontaneous activation is expected to be negligible.

The drop in the discrete noise component indicates that the A1 chromophore and the opsin form a pigment that is less susceptible to thermal isomerization than that formed by the A2 chromophore with the same opsin. Qualitatively, this is in line with several earlier studies. Williams & Milby (1968) found that the thermal decomposition of bullfrog A2 rod pigment in solution was 10 times faster than that of the corresponding A1 pigment. However, the

molecular mechanism of decomposition in solution may be quite different from that underlying pigment activation *in situ*. More directly comparable are the results of Donner *et al.* (1990), who measured dark noise in rods isolated from A2- or A1-dominated fields of the bullfrog retina. They estimated that the thermal activation rate of the A2 pigment was at least 10-fold higher than that of A1 pigment per molecule. Kefalov *et al.* (2005) found an 11-fold decrease in the rate of spontaneous activations in salamander L-cones upon substituting the A2 by the A1 chromophore (see also Acknowledgements).

As such, our results are consistent with these (lower-limit) estimates, but our experiments have a higher resolving power, allowing us to set the lower limit for the ratio of thermal activation probabilities in A2 *versus* A1 pigment as high as 36-fold. This is of considerable significance for the interpretation of molecular mechanisms as well as for considerations of visual sensitivity.

We finally wish to comment on a hypothetical alternative explanation of our main result. Could the decrease in discrete noise be a consequence of bleaching and regenerating *per se* rather than the A2 → A1 chromophore switch? We think this is extremely unlikely for (at least) four reasons. Firstly, we performed control experiments on toad (*Bufo marinus*) rods, bleaching 90% of their pure A1 pigment and regenerating with the same (A1) chromophore. The estimated dark event rates in these experiments fell in the range 0.015–0.030 $Rh^* s^{-1}$ (21°C) both before and after bleaching and regeneration, consistent with the mean value (0.021 $Rh^* s^{-1}$ at 20°C) reported by Baylor *et al.* (1980) for the same species. Secondly, bleaching small fractions (0.02–3%) of the rhodopsin in toad rods has been found to cause a transient *increase* in the rate of photon-like dark events, apparently due to bleaching products of rhodopsin (e.g. metarhodopsin III) being converted back to Rh^* (metarhodopsin II) (Lamb, 1980; Leibrock *et al.* 1994, 1998). This (fully reversible) effect of bleaching *per se* is obviously opposite to the change observed here after bleaching native salamander rods and regenerating with the A1 chromophore. On the other hand, any hypothetical after-effect specific to *strong* bleaches, acting to decrease discrete noise in the final state after regeneration (through some change in the physiology of the cell) would be expected to affect fractional sensitivity or the shape of the SQR as well. Thirdly, we find a clear correlation of final-state event rate with the fraction of A2 pigment remaining (see Fig. 6), which would be enigmatic if the noise did not depend on the chromophore. Fourthly, the change we find upon bleaching A2 and regenerating with the A1 chromophore is qualitatively consistent with the difference found by Donner *et al.* (1990) when comparing dark event rates of bullfrog A2 and A1 rods that had not been bleached.

Spectral tuning and the stability of visual pigments

The chromophore switch (A2 → A1) blue-shifted λ_{max} by 26 nm and decreased the thermal activation rate of the pigment by more than 30-fold. The coupling of these two changes is consistent with a hypothesis proposed by Barlow (1957) stating that the energy (E_a) needed for activation of a pigment is inversely proportional to λ_{max}; hence larger λ_{max} indicates lower E_a and thus a higher probability for activation by thermal energy alone. In his original formulation of this general idea, Barlow (1957) assumed that the fraction of visual pigment molecules on thermal energy levels $> E_a$ is given by the Boltzmann distribution and E_a corresponds to the energy of a light quantum at λ_{max}. An approximately 120-fold increase in thermal activations is predicted when λ_{max} shifts, as here, from 502 (A1) to 528 nm (A2). The prediction falls well within our 95% confidence range for $f_{mol,A2}/f_{mol,A1}$ (see the last two paragraphs of Results).

By contrast, when comparisons are made across different species of rods (as well as cones) with different λ_{max}, the average dependence between thermal event rate and λ_{max} has been found to be much shallower than predicted by Barlow's simple formulation. Figure 7 reproduces the available rod data, including our present

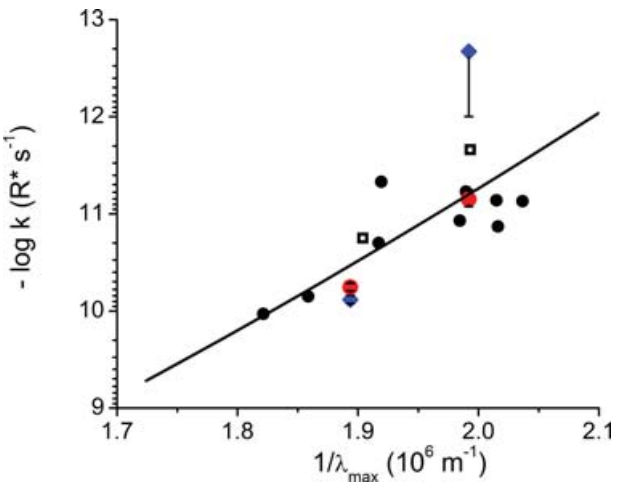

Figure 7. Dark event rates per molecule of visual pigment in 11 species of rods
Molecular dark event rates are plotted against the reciprocal of the wavelength of peak absorbance ($1/\lambda_{max}$). The Briggsian logarithm of the rate constant (k) is plotted as a function of $1/\lambda_{max}$. The molecular rate constants have been corrected for differences in cell dimensions and temperature (all have been recalculated to 21°C; see details in Ala-Laurila *et al.* 2004*a*). The black symbols have been re-plotted from Ala-Laurila *et al.* (2004*a*). Red circles, native-state and final-state estimates for salamander rods from the present work; blue diamonds, present estimates for pure A1 and pure A2 pigment of salamander. The open squares show estimates for rods from the A2-dominated (dorsal) and A1-dominated (ventral) fields of bullfrog retina (Donner *et al.* 1990). Error bars are S.E.M. The black continuous line shows the original fit of the multimodal model of Ala-Laurila *et al.* (2004*a*) to the black data points.

estimates for the pure A1 and pure A2 pigment of salamander (blue diamonds). The general trend of the earlier data was well fitted by a modified theory proposed by Ala-Laurila *et al.* (2004*a*; continuous line in figure), which takes into account that the thermal energy of the pigment molecule is distributed on a large number of vibrational modes (cf. Hinshelwood, 1933). While the present estimate for salamander A2 pigment (the blue diamond at $1/\lambda_{max} \approx 1.9 \times 10^6$ m^{-1}) is roughly in line with this model and most other pigments, our A1 estimate is clearly an outlier. This will require further investigation. At this stage, two points should be noted, however. First, the 95% confidence interval of our (extrapolated) rate of thermal events in pure A1 pigment spans two orders of magnitude and thus the data cannot strongly differentiate between models. Second, in studies of photoactivation energies (E_a) of several visual pigments, it has been found that λ_{max} shifts due to differing chromophores are associated with larger E_a shifts (i.e. more in line with Barlow, 1957 prediction) than are λ_{max} shifts due to differing opsins (Ala-Laurila *et al.* 2004*b*). One may argue that an opsin that has to form a reasonably noise-free pigment with the relatively unstable A2 chromophore must be evolutionarily tuned to be particularly stabilizing. This would apply to the opsins of salamanders and frogs, but not to those of toads (Muntz & Reuter, 1966), and would become evident as exceptional thermal stability of the A1 form of the pigment (cf. Donner *et al.* 1990).

We would finally like to point out that the correlation between λ_{max} and dark event rates predicted by theory and empirically exemplified in Fig. 7 relates specifically to the dark-adapted steady state. It does not exclude quite different effects in other conditions. Corson *et al.* (1990) found greatly increased light-like noise in salamander red rods after bleaching and regenerating the pigment with 4-hydroxy retinal (a chromophore common in insect pigments), although the new pigment was relatively blue-shifted ($\lambda_{max} = 470$ nm). However, this noise was observed only transiently after light exposure and is not comparable to discrete noise measured in the dark-adapted steady state.

The chromophore switch and absolute visual sensitivity

Switching between A1 and A2 chromophores in the same opsin occurs naturally in many fish and amphibian species in connection with seasonal changes, migration or metamorphosis (for recent review, see Temple *et al.* 2006). Visual detection is a signal/noise discrimination task, and functional consequences must therefore be viewed under the double perspective of spectral tuning and noise control. For achromatic rod vision, the pigment that allows the highest quantum catch is always most beneficial in somewhat stronger illumination, but at very low light levels, the thermal dark events may become limiting (Jokela-Määttä *et al.* 2007).

In amphibians and humans, the threshold intensity for seeing an extended object in darkness has been found to lie roughly where the rate of photoisomerizations from the object coincides with the estimated rate of rod dark events in the retinal area covered by the image of the object. In the toad *Bufo bufo* at 15°C, threshold corresponds to *ca* 0.02 Rh* s^{-1} in each rod covered by the image (Aho *et al.* 1988, 1993), while the dark event rate in the same species at the same temperature is *ca* 0.01 Rh* s^{-1} (Fyhrquist *et al.* 1998; Firsov *et al.* 2002). The human threshold (at body temperature, 37°C) in the same detection task as performed by the toads also corresponded to *ca* 0.01 Rh* s^{-1} (Aho *et al.* 1988), close to the rate of dark events per rod estimated from psychophysical data (Barlow, 1956; Donner, 1992) as well as from discrete dark noise in macaque cones (Baylor *et al.* 1984). Yet it should be noted that in terms of photoisomerizations per *unit retinal area* (Rh* mm^{-2} s^{-1}), the human threshold is more than 10 times higher than the toad threshold, since peak rod density in humans is *ca* 160 000 mm^{-2}, but only *ca* 12 000 mm^{-2} in toad (Østerberg, 1935; Aho *et al.* 1993). Of course the same difference holds for the dark event rates per unit retinal area. At present, this empirical generalization has no straightforward mechanistic explanation in terms of signal-to-noise ratio at threshold. Assuming that it is valid, however, a hypothetical switch from 100% A1 to 100% A2 in a salamander rod, increasing the estimated dark event rate from $\leq$ 0.01 Rh* s^{-1} to *ca* 0.3 Rh* s^{-1}, would pay off only if quantum catch were thereby increased by at least 30-fold. Given the 1.42 times lower photosensitivity of the A2 pigment, retinal illumination would have to increase by 40- to 50-fold to retain the same threshold ratio of photoisomerizations to thermal isomerizations in the presence of pure A2 pigment as in the presence of pure A1 pigment.

Size of the SQR. In 3 cells out of 5 we observed an increase in the SQR amplitude and integration time in the final state compared with the native state (cf. Fig. 3*C*). This might suggest that the thermal events occurring at a rate of *ca* 1 event per integration time may keep the native (A2) cell in a slightly 'light-adapted' state compared with the final state, where the 'intrinsic background light' is 8 times dimmer. Baylor *et al.* (1980) concluded that thermal activation of rhodopsin is unlikely to play a significant role in desensitizing the transduction mechanism in darkness in toad rods, where the rate of discrete dark events is only about one per 20 integration times. Even so, these authors did find an inverse correlation between SQR amplitude and integration time in darkness, suggesting that the sensitivity and time scale of the transduction mechanism are indeed regulated in darkness by the same variable

operative in background light. However, we cannot exclude the possibility that the slower response and increased amplitude in the final state may be side-effects due, e.g. to unspecific loss of mechanisms for response cut-off over the course of the long experiments, rather than expressive of normal adaptation.

Whenever randomly occurring events identical to the SQR constitute the dominant noise component, the size of the SQR is irrelevant for the signal-to-noise ratio of vision. In the native state, this may approximately be the case, since the discrete noise constituted 70% of the total noise power. In a pure A1 rod, however, the continuous noise (which was unaffected by chromophore change) is predicted to be the dominant component of dark variance. In such a case light detection would benefit greatly from a larger SQR.

Taken together, we have shown in this paper that the A1 chromophore forms *in situ* a much more stable pigment with the red rod opsin in the Rh1 pigment family than the A2 chromophore. We estimate that the thermal stability of the 502 nm A1 pigment is over 36-fold greater than its 528 nm A2 pair. This observation is in line with a theory according to which spectral tuning towards shorter wavelengths is coupled with a decreased rate of spontaneous activations (Barlow, 1957; Ala-Laurila *et al.* 2004*a*). In addition, the larger and slower single-photon response in the final (A1) state is consistent with the idea that spontaneous activations that occur at a rate of nearly one per integration time in the native (A2) state can light-adapt rods.

References

Aho AC, Donner K, Helenius S, Olesen Larsen L & Reuter T (1993). Visual performance of the toad (*Bufo bufo*) at low light levels: retinal ganglion cell responses and prey-catching accuracy. *J Comp Physiol [A]* **172**, 671–682.

Aho AC, Donner K, Hyden C, Larsen LO & Reuter T (1988). Low retinal noise in animals with low body temperature allows high visual sensitivity. *Nature* **334**, 348–350.

Ala-Laurila P, Donner K & Koskelainen A (2004*a*). Thermal activation and photoactivation of visual pigments. *Biophys J* **86**, 3653–3662.

Ala-Laurila P, Pahlberg J, Koskelainen A & Donner K (2004*b*). On the relation between the photoactivation energy and the absorbance spectrum of visual pigments. *Vision Res* **44**, 2153–2158.

Barlow HB (1956). Retinal noise and absolute threshold. *J Opt Soc Am* **46**, 634–639.

Barlow HB (1957). Purkinje shift and retinal noise. *Nature* **179**, 255–256.

Baylor DA & Hodgkin AL (1973). Detection and resolution of visual stimuli by turtle photoreceptors. *J Physiol* **234**, 163–198.

Baylor DA, Hodgkin AL & Lamb TD (1974). The electrical response of turtle cones to flashes and steps of light. *J Physiol* **242**, 685–727.

Baylor DA, Lamb TD & Yau KW (1979*a*). The membrane current of single rod outer segments. *J Physiol* **288**, 589–611.

Baylor DA, Lamb TD & Yau KW (1979*b*). Responses of retinal rods to single photons. *J Physiol* **288**, 613–634.

Baylor DA, Matthews G & Yau KW (1980). Two components of electrical dark noise in toad retinal rod outer segments. *J Physiol* **309**, 591–621.

Baylor DA, Nunn BJ & Schnapf JL (1984). The photocurrent, noise and spectral sensitivity of rods of the monkey *Macaca fascicularis*. *J Physiol* **357**, 575–607.

Bodoia RD & Detwiler PB (1985). Patch-clamp recordings of the light-sensitive dark noise in retinal rods from the lizard and frog. *J Physiol* **367**, 183–216.

Cornwall MC, Jones GJ, Kefalov VJ, Fain GL & Matthews HR (2000). Electrophysiological methods for measurement of activation of phototransduction by bleached visual pigment in salamander photoreceptors. *Meth Enzymol* **316**, 224–252.

Corson DW, Cornwall MC, MacNichol EF, Mani V & Crouch RK (1990). Transduction noise induced by 4-hydroxy retinals in rod photoreceptors. *Biophys J* **57**, 109–115.

Crouch RK, Kefalov V, Gartner W & Cornwall MC (2002). Use of retinal analogues for the study of visual pigment function. *Meth Enzymol* **343**, 29–48.

Dartnall HJ (1968). The photosensitivities of visual pigments in the presence of hydroxylamine. *Vision Res* **8**, 339–358.

Dartnall HJA (1972). Photosensitivity. In *Handbook of Sensory Physiology*, vol. VII/1, *Photochemistry of Vision*, ed. Dartnall HJA, pp. 122–145. Springer, Berlin-Heidelberg-New York.

Dartnall HJ & Lythgoe JN (1965). The spectral clustering of visual pigments. *Vision Res* **5**, 81–100.

Donner K (1992). Noise and the absolute thresholds of cone and rod vision. *Vision Res* **32**, 853–866.

Donner K, Firsov ML & Govardovskii VI (1990). The frequency of isomerization-like 'dark' events in rhodopsin and porphyropsin rods of the bull-frog retina. *J Physiol* **428**, 673–692.

Estevez ME, Ala-Laurila P, Crouch RK & Cornwall MC (2006). Turning cones off: the role of the 9-methyl group of retinal in red cones. *J Gen Physiol* **128**, 671–685.

Firsov ML, Donner K & Govardovskii VI (1994). Response univariance in bull-frog rods with two visual pigments. *Vision Res* **34**, 839–847.

Firsov ML, Donner K & Govardovskii VI (2002). pH and rate of 'dark' events in toad retinal rods: test of a hypothesis on the molecular origin of photoreceptor noise. *J Physiol* **539**, 837–846.

Fyhrquist N, Govardovskii VI, Leibrock C & Reuter T (1998). Rod pigment and rod noise in the European toad *Bufo bufo*. *Vision Res* **38**, 483–486.

Govardovskii VI, Fyhrquist N, Reuter T, Kuzmin DG & Donner K (2000). In search of the visual pigment template. *Vis Neurosci* **17**, 509–528.

Hárosi FI (1975). Absorption spectra and linear dichroism of some amphibian photoreceptors. *J Gen Physiol* **66**, 357–382.

Hárosi FI (1994). An analysis of two spectral properties of vertebrate visual pigments. *Vision Res* **34**, 1359–1367.

Hinshelwood CN (1933). *The Kinetics of Chemical Change in Gaseous Systems*. Clarendon Press, Oxford, UK.

Holcman D & Korenbrot JI (2005). The limit of photoreceptor sensitivity: molecular mechanisms of dark noise in retinal cones. *J Gen Physiol* **125**, 641–660.

Jokela-Määttä M, Smura T, Aaltonen A, Ala-Laurila P & Donner K (2007). Visual pigments of Baltic Sea fishes of marine and limnic origin. *Vis Neurosci* **24**, 389–398.

Jones GJ (1995). Light adaptation and the rising phase of the flash photocurrent of salamander retinal rods. *J Physiol* **487**, 441–451.

Jones GJ (1998). Membrane current noise in dark-adapted and light-adapted isolated retinal rods of the larval tiger salamander. *J Physiol* **511**, 903–913.

Kefalov VJ, Crouch RK & Cornwall MC (2001). Role of noncovalent binding of 11-*cis*-retinal to opsin in dark adaptation of rod and cone photoreceptors. *Neuron* **29**, 749–755.

Kefalov V, Fu Y, Marsh-Armstrong N & Yau KW (2003). Role of visual pigment properties in rod and cone phototransduction. *Nature* **425**, 526–531.

Kefalov VJ, Fu Y & Yau KW (2005). Higher Rate of Thermal Activation of Red Cone Pigments With 11-cis A2 Compared to 11-cis A1 Retinal as Chromophore. *Invest Ophthalmol Vis Sci* **46**, E-Abstract 2264.

Lamb TD (1980). Spontaneous quantal events induced in toad rods by pigment bleaching. *Nature* **287**, 349–351.

Lamb TD & Simon EJ (1977). Analysis of electrical noise in turtle cones. *J Physiol* **272**, 435–468.

Leibrock CS, Reuter T & Lamb TD (1994). Dark adaptation of toad rod photoreceptors following small bleaches. *Vision Res* **34**, 2787–2800.

Leibrock CS, Reuter T & Lamb TD (1998). Molecular basis of dark adaptation in rod photoreceptors. *Eye* **12**, 511–520.

Lythgoe JN (1988). Light and vision in the aquatic environment. In *Sensory Biology of Aquatic Animals*, ed. Atema J, Fay RR, Popper AN & Tavolga WN, pp. 57–82. Springer, Berlin.

MacNichol EF Jr (1978). A photon-counting microspectrophotometer for the study of single vertebrate photoreceptor cells. In *Frontiers of Visual Science*, ed. Cool SJ & Smith EL, pp. 194–208. Springer, Berlin.

Makino CL, Groesbeek M, Lugtenburg J & Baylor DA (1999). Spectral tuning in salamander visual pigments studied with dihydroretinal chromophores. *Biophys J* **77**, 1024–1035.

Muntz WA & Reuter T (1966). Visual pigments and spectral sensitivity in *Rana temporaria* and other European tadpoles. *Vision Res* **6**, 601–618.

Østerberg G (1935). Topography of the layer of rods and cones in the human retina. *Acta Ophthalmologica* **13**, 1–103.

Rieke F (2000). Mechanisms of single-photon detection in rod photoreceptors. *Meth Enzymol* **316**, 186–202.

Rieke F & Baylor DA (1996). Molecular origin of continuous dark noise in rod photoreceptors. *Biophys J* **71**, 2553–2572.

Rieke F & Baylor DA (2000). Origin and functional impact of dark noise in retinal cones. *Neuron* **26**, 181–186.

Ritter E, Elgeti M, Hofmann KP & Bartl FJ (2007). Deactivation and proton transfer in light-induced metarhodopsin II/metarhodopsin III conversion: a time-resolved Fourier transform infrared spectroscopic study. *J Biol Chem* **282**, 10720–10730.

Sampath AP & Baylor DA (2002). Molecular mechanism of spontaneous pigment activation in retinal cones. *Biophys J* **83**, 184–193.

Schneeweis DM & Schnapf JL (2000). Noise and light adaptation in rods of the macaque monkey. *Vis Neurosci* **17**, 659–666.

Schwartz EA (1977). Voltage noise observed in rods of the turtle retina. *J Physiol* **272**, 217–246.

Temple SE, Plate EM, Ramsden S, Haimberger TJ, Roth WM & Hawryshyn CW (2006). Seasonal cycle in vitamin A1/A2-based visual pigment composition during the life history of coho salmon (*Oncorhynchus kisutch*). *J Comp Physiol A Neuroethol Sens Neural Behav Physiol* **192**, 301–313.

Tsina E, Chen C, Koutalos Y, Ala-Laurila P, Tsacopoulos M, Wiggert B, Crouch RK & Cornwall MC (2004). Physiological and microfluorometric studies of reduction and clearance of retinal in bleached rod photoreceptors. *J Gen Physiol* **124**, 429–443.

Vu TQ, McCarthy ST & Owen WG (1997). Linear transduction of natural stimuli by dark-adapted and light-adapted rods of the salamander, *Ambystoma tigrinum*. *J Physiol* **505**, 193–204.

Williams TP & Milby SE (1968). The thermal decomposition of some visual pigments. *Vision Res* **8**, 359–367.

Acknowledgements

We thank Dr Maureen Estevez for skilful help and advice in the preparation of retinoid solutions as well as wonderful encouragement during this study. We thank Mr Howard I. Cohen for upgrading and improving the microspectrophotometer originally designed by Edward MacNichol, and Professor Tom Reuter for commenting on the manuscript. An unpublished study by Y. Fu, V. Ketalov, D.–G Luo, T. Xue and K.–W Yau using transgenic mice has shown that the spontaneous isomerization rate of human red cone pigment with A2 chromphore is $\sim$40 times higher than with A1 chromophore (K.–W. Y., personal communication), thus similar to our finding for salamander rhodopsin. This study was supported by a grant from Helsingin Sanomain 100-vuotissäätiö (to P. Ala-Laurila), from the Academy of Finland (grant 206221) and Societas Scientiarum Fennica (to K. Donner) and NIH grants EY-01157 (to M. C. Cornwall) and EY-04939 (to R. K. Crouch), EY-14793 (MUSC) and C06 grant R015455 from the Extramural Research Facilities Program of the National Center for Research Resources; an unrestricted grant to the Department of Ophthalmology at Medical University of South Carolina from Research to Prevent Blindness (RPB, New York). R. K. Crouch is a RPB Senior Scientific Investigator.